

Water Conservation & Management (WCM)

DOI: http://doi.org/10.26480/wcm.01.2025.93.104



ISSN: 2523-5672 (Online) CODEN: WCMABD

RESEARCH ARTICLE

EVALUATING CROP WATER REQUIREMENTS: A CASE STUDY OF DATE PALMS IN WATER-SCARCE JORDAN

Shadia Alqudaha, Ayman Suleimana, Motasem Y.D. Alazaizab,*, Heba Al-Jawaldeha

- ^aDepartment of Land, Water, and Environment, School of Agriculture, The University of Jordan, Amman 11942, Jordan
- ^bDepartment of Civil and Construction Engineering, College of Engineering (COE), A'Sharqiyah University (ASU), Ibra, Oman.
- *Corresponding Author Email: my.azaiza@gmail.com

This is an open access journal distributed under the Creative Commons Attribution License CC BY 4.0, which permits unrestricted use, distribution, and reproduction in any medium, provided the original work is properly cited

ARTICLE DETAILS

Article History:

Received 23 December 2024 Revised 03 January 2025 Accepted 18 January 2025 Available online 14 February 2025

ABSTRACT

The rapid expansion of date palm cultivation in Jordan presents significant challenges related to water management, particularly as the region faces increasing water scarcity. This study addresses the urgent need for precise estimation of crop water requirements by evaluating the actual daily evapotranspiration (ETa) of date palms. We employed the Analytical Atmospheric Land Radiation Measurement (ALARM) model and compared its performance with the Evapotranspiration Look (ETLook) model to determine their effectiveness in capturing the water needs of these crops. Utilizing six satellite images from Landsat 8 and 9, we conducted our analysis over a period from February 9 to May 15, 2024. The results indicated that the ALARM model produced ETa values ranging from 2.58 mm/day to 5.23 mm/day, with an average of approximately 4.23 mm/day. In contrast, the ETLook model, which relies on data from the WaPOR portal and incorporates MODIS and PROBA-V satellite information, yielded significantly lower estimates, with values between $0.975 \ \text{mm/day}$ and a maximum of 2.125 mm/day This discrepancy suggests that the ETLook model may adopt a conservative approach, potentially underestimating the water requirements during critical growth phases, which could adversely impact crop health and yield. Furthermore, the average root mean square error (RMSE) between the two models was approximately 2.7 mm/day, indicating variability in their performance. The findings emphasize the ALARM model's superiority for detailed assessments in heterogeneous landscapes, making it particularly suitable for optimizing irrigation strategies tailored to the specific needs of date palms. Conversely, the ETLook model may be better suited for broader regional assessments, providing a more generalized view of water consumption. In conclusion, integrating both models can enhance water use efficiency and support sustainable agricultural practices in water-scarce environments. By improving our understanding of ETa dynamics in date palm cultivation, this study contributes valuable insights for effective water resource management and the long-term sustainability of agricultural systems in Jordan and similar arid regions

KEYWORDS

ALARM, Crop Water Requirement, Date palm, ETLook, Actual Evapotranspiration (ETa), Irrigation, Jordan valley, Lysimeters; Remote Sensing.

1. Introduction

Sustainable water usage has become a critical issue in regions experiencing water scarcity, affecting agriculture and various other sectors (Sahoo and Goswami, 2024). The increasing demand for water, coupled with declining quality of surface and groundwater, has intensified competition among different sectors for limited resources (Sahoo and Goswami, 2024). Increasing world pollution, overuse of groundwater sources, utilizing water for diverse applications, and decreasing rainfall due to climate change led to water scarcity in regions with high rainfall as well as arid areas (Asadi and Karami, 2020; Chen et al., 2024). Water scarcity is defined not only by the availability of water for economic and social purposes but also by the requirements of both natural and man-made ecosystems (Acharya et al., 2021; Koebela and Simpson, 2023; Hamaideh et al., 2024). The notion of scarcity also encompasses water quality, as inadequate water resources are either inaccessible or of little value in both human and natural systems (Hamaideh et al., 2024). Furthermore, the concept of scarcity encompasses water quality; inadequate resources may be

inaccessible or of little value to human and ecological systems. Consequently, effective measures are urgently needed to conserve natural resources, prevent waste, and maintain water quality (Hamaideh et al., 2024).

Irrigation, as one of the most significant uses of water globally, faces increasing pressure from various sectors, including agriculture, urban development, industry, and tourism (Hamaideh et al., 2024). This heightened competition for water resources is further intensified by climate change, which poses serious threats to vulnerable agricultural sectors (Slama et al., 2019). While irrigated agriculture is known to be the highest consumer of water worldwide and has faced criticism for generating waste and compromising water quality, it remains a vital sector that sustains the livelihoods of many rural populations and contributes substantially to global food production (Perry and Praskievicz, 2017; Slama et al., 2019). To address the multifaceted challenges posed by water scarcity, numerous studies have sought innovative water management strategies aimed at expanding water utilization and enhancing both crop

Quick Response Code

Access this article online



Website: www.watconman.org DOI:

10.26480/wcm.01.2025.93.104

yields and farmers' incomes (Al Zayed et al., 2016; Atasever and Ozkan, 2018).

As the global population continues to grow, there is an urgent need to increase food production while protecting the environment. Modern agricultural practices must find ways to increase crop productivity (Al Zayed et al., 2016). Precision agriculture offers a promising solution by employing advanced technologies and methodologies for more effective land and crop management. This can improve production, protect the environment, and raise the quality of agricultural products. Precision agriculture is especially relevant in arid and semi-arid regions, where climate change and rising water salinity present serious challenges (Costa et al., 2019; Kalua et al., 2020). The most significant consumer of water in agriculture is cropland irrigation, making it crucial to develop reliable methods for measuring water consumption by crops to ensure sustainable management practices (Tan et al., 2018). Understanding the amount of water lost through evapotranspiration (ET) can provide insights into water demand and land productivity, establishing crop-specific relationships between ET and yield (Reints et al., 2020). Yield, as a critical indicator of crop response to water management, is vital for rural development and national food security. Therefore, quantifying ET at the field level is essential for maximizing land productivity while minimizing water losses (Reints et al., 2020).

Jordan, located in the eastern Mediterranean and covering approximately 90,000 km², faces significant challenges related to water scarcity. With a population of around 11 million, the country's diverse terrain includes features such as the Rift Valley, highlands reaching up to 1,600 meters above sea level, desert regions, and the Dead Sea, which sits at 426 meters below sea level in 2010 (Trottier et al., 2016; Ayasrah and Hanandeh, 2024). The climate in Jordan varies significantly; the western regions experience a Mediterranean climate characterized by hot, dry summers and mild, wet winters, while the Jordan Rift Valley and Aqaba have subtropical climates with hot summers and warm winters (Trottier et al., 2020; Jamrah et al., 2024). The favorable environmental conditions in the Jordan Valley and Aqaba have made date palm cultivation increasingly popular among farmers, as date palms require less irrigation than other crops and are well-suited to hot, saline soils (Hodgson, 2015; Al-Khayri and Naik, 2017; Bani Ataa et al., 2024). To achieve sustainable irrigation management, it is crucial to determine the crop water requirements of date palms through either ground-based or remotely sensed methods. The inadequate estimation of daily actual evapotranspiration (ETa) for date palm trees has led to inefficient irrigation practices and significant water loss in the region.

Crop water demand is defined as the volume of water applied to an agricultural field to meet the needs of the crops' actual ETa (Ayyad et al., 2019; Chakroun et al., 2023; Kumar and Hamouda, 2025). Accurate estimation of ETa is fundamental for agricultural water management, enabling effective water resource planning, allocation, and efficiency studies. Various field-based methods have been developed to measure ETa directly, including lysimeter systems and the eddy covariance method (Chakroun et al., 2023). However, these approaches often suffer from limitations related to localized measurement and the availability of meteorological data, particularly in remote areas. Ground and remote sensing methods are two approaches used to collect environmental information, so the ground methods involve physically going to a site and collecting data directly (Meza et al., 2025). This could include taking measurements with instruments, conducting surveys, or taking soil, water, or air samples (Chakroun et al., 2023). While these methods tend to be more accurate than remote sensing approaches, they can also be timeconsuming and costly (Chakroun et al., 2023).

Remote sensing methods for estimating ET, such as Surface Energy Balance Algorithms for Land (SEBAL) (Elkatoury et al., 2024), Evapotranspiration Look (ETLOOK) (Bastiaanssen et al., 2012), Metric (Sejine and Anane, 2024), and Analytical Land-Atmosphere Radiometer Model (ALARM) (Suleiman and Al-Bakri, 2011), offer alternative ways to gather environmental data over larger areas, though they may sacrifice some accuracy compared to ground-based techniques. These methods leverage satellite data to estimate ET and monitor water use in agricultural settings (Atasever and Ozkan, 2018). For instance, SEBAL utilizes satellite data to calculate surface energy fluxes, including ET, and has been widely adopted for monitoring irrigation efficiency and crop yield forecasting (Suleiman and Al-Bakri, 2011; Atasever and Ozkan, 2018). Additionally, SEBAL has been applied to estimate urban areas' water consumption and monitor the effects of land-use changes on the environment (Kumar and Hamouda, 2025). SEBAL requires input data to estimate the surface energy balance components. The accuracy of SEBAL outputs depends on the input data's accuracy, so the data's quality must be carefully controlled (Costa et al.,

2019). Similarly, ALARM and ETLook employ atmospheric data and satellite imagery to estimate ET, providing crucial insights for water management across extensive regions (Bastiaanssen et al., 2012; Owaneh and Suleiman, 2018). ALARM is remote sensing method that estimates surface energy fluxes using atmospheric data, employing energy equilibrium algorithms to derive instantaneous and daily ET values based on physical and experimental relationships using satellite imagery and low-ground observational data (Suleiman and Crago, 2002; Owaneh and Suleiman, 2018). To estimate ET using ALARM, remotely sensed vegetation index and canopy temperature and weather parameters such as surface temperature, net radiations, soil heat flux, and sensible heat flux. Finally, calculations are made for the instantaneous flux and the amount of daily ET (Bastiaanssen et al., 2012).

Similarly, ETLook estimates ET using satellite data and weather information, making it a valuable tool for monitoring water use and drought conditions across large regions. ETLook is commonly used to monitor water use in agricultural areas and assess drought conditions (Suleiman and Al-Bakri, 2011). Using remote sensing data, the ETLook algorithm is a computational method used to estimate ET over large regions. It utilizes data from the Moderate Resolution Imaging Spectroradiometer (MODIS) sensor, which captures visible and nearinfrared light, and the Advanced Microwave Scanning Radiometer for Earth Observing System (AMSR-E) sensor, which provides soil moisture estimates (Bastiaanssen et al., 2012). The ETLook algorithm solves the Penman-Monteith equation separately for soil and vegetation, which allows for the partitioning of ET into transpiration and evaporation (Pelgrum et al., 2012). To estimate ET, the algorithm considers various environmental factors such as solar radiation, air temperature, wind speed, and relative humidity. It can provide estimates of ET daily or weekly, and it has been used in various regions worldwide, including Australia, China, and the Indus basin (Pelgrum et al., 2012). The ETLook algorithm has several advantages over other methods for estimating ET, including its ability to work with low-resolution soil moisture data and its scalability over large areas. It is useful for various applications, including water management, drought monitoring, and crop yield forecasting (Bastiaanssen et al., 2012).

In this study, the daily ETa of date palm trees was estimated using the ETLook and ALARM algorithms, with results compared against the water balance method. The increasing adoption of these algorithms reflects their $capability \ to \ estimate \ ET\ rates\ independently\ of\ soil\ conditions, crop\ types,$ and management practices. The main objectives of this research are to provide a cost-effective and time-efficient means of determining the precise water requirements of date palms, minimize water wastage, and enhance irrigation efficiency. Furthermore, the study aims to address the lack of awareness regarding crop water needs, which has led to inadequate irrigation management practices among farmers, resulting in significant water loss and additional pressure on both surface and groundwater resources in the region. While previous studies have successfully utilized the ALARM model to estimate ET for crops such as potatoes and alfalfa in the Jordan Valley, research specifically addressing ET for date palms remains limited. This study seeks to fill this knowledge gap by delivering a robust analysis of the daily water requirements for date palms through remote sensing data, providing an improved approach to crop water estimation compared to traditional point measurements. By evaluating the performance of the ETLook and ALARM algorithms against the widely accepted water balance equation and incorporating comparisons of ground weather data with NASA Power data, this research endeavors to contribute valuable insights into the potential of remote sensing in agricultural water management. Ultimately, the findings hold significant implications for promoting efficient and sustainable water management practices within the context of Jordan's pressing water scarcity challenges.

2. MATERIALS AND METHODS

The methodology employed in this study involved estimating the actual daily crop water requirements for date palm trees using the ETLook and ALARM models. Remote sensing data were acquired from the Landsat 8 satellite, which provides regular imagery of the study area. These images were utilized to derive key metrics, including surface canopy temperature and the vegetation leaf area index (LAI) of the date palms. Additionally, meteorological data—such as air temperature, humidity, wind speed, and solar radiation—were sourced from a nearby weather station and NASA's power data. The ALARM model was specifically applied to estimate the ETa for the date crops, utilizing an energy balance equation that calculates ETa based on the energy inputs and outputs at the land surface.

2.1. Study Area

The Jordan Valley is one of the oldest and most significant agricultural centers in Jordan (Dhehibi et al., 2017). This study was conducted at the AL-Quafil Farms, located in the central Jordan Valley at a latitude of 32° 5'5" N and a longitude of 35° 35'51" E, at an altitude of 230 meters below mean sea level. The site was specifically chosen within a field of date palm trees, as this location is recognized for its agricultural prosperity and extensive, well-defined farmlands, making it a principal agricultural hub in Jordan. The selected farm operates under the supervision of the Al-Quafil Agricultural Research Center, which ensures effective irrigation management and maintains optimal soil conditions for plant growth.

The farm covers an area of 65 dunams, with approximately 1,080 date palm trees irrigated via a drip system. The palm trees are around 7 to 8 years old and have an average height of 5.25 meters, with a spacing of 8 meters between each tree, resulting in a density of about 150 trees per hectare. For this study, a total area of 40 dunams planted with Medjoul date palms was utilized, divided into four pixels, as illustrated in Figure 1, with each pixel measuring 100 by 100 meters. These pixels were further subdivided into sub-pixels measuring 30 by 30 meters. The analysis focused on the sub-pixels labeled P1, P2, P3, and P4, in accordance with the resolution of Landsat 8 imagery.

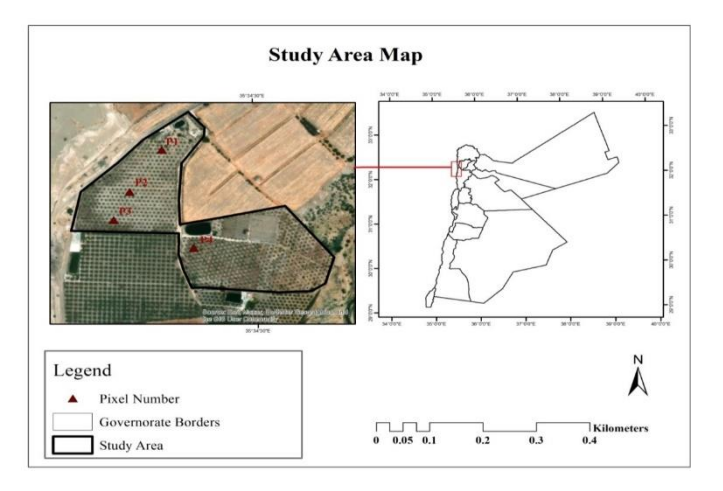


Figure 1: Location map of study area.

2.2 Meteorological Data

Meteorological data for the study period were collected from the Dair Alla Meteorological Station and NASA Power Station. The recorded parameters included average daily solar radiation (MJ/m² per day), wind speed (m/s), maximum and minimum daily air temperatures (°C), and average, maximum, and minimum relative humidity (%). These values were utilized to calculate ETa. Additionally, specific weather parameters—hourly air temperature, wind speed, and solar radiation—were recorded during the satellite overpass, which are essential for the ALARM model. Daily net solar radiation was also necessary for converting instantaneous ETa into daily FTa

2.3 Satellite Images

This study utilized six Landsat 8 and 9 images to monitor the growth period of date trees, spanning from February 9 to May 15, 2024. The inclusion of Landsat 9 images was necessary due to the unavailability of Landsat 8 images for every 8-day interval during this period. The specifications of the satellite images used are detailed in Table 1. These images were crucial for estimating the ETa of the date trees within the study area.

Table 1: Landsat images used during the study period.							
N o	ID	Date Acquir ed	Time of overp ass	Clo ud Cov er %			
1	LC08_L1TP_174038_20240209_202 40213_02_T1	Februa ry 9, 2024	08:10: 56	10.3 7			
2	LC08_L1TP_174038_20240312_202 40401_02_T1	March 17, 2024	08:10: 41	0.43			

Table 1(Cont.): Landsat images used during the study period.							
3	LC08_L1TP_174038_20240328_202 40410_02_T1	March 28, 2024	08:10: 25	1.80			
4	LC09_L1TP_174038_20240405_202 40405_02_T1	April 5, 2024	08:10: 50	0.17			
5	LC09_L1TP_174038_20240421_202 40421_02_T1	April 21, 2024	08:10: 33	5.78			
6	LC08_L1TP_174038_20240515_202 40521_02_T1	May 15, 2024	08:09: 57	2.96			

All images utilized in this study were downloaded from https://earthexplorer.usgs.gov and are free from geometric errors, with a cloud cover percentage of less than 10%. The six high-resolution remote sensing images from the Landsat 8 and Landsat 9 satellites were processed to determine land surface temperature (LST), surface albedo, and estimate LAI. Landsat 8 captures data across 11 spectral bands using two distinct sensors: The Operational Land Imager (OLI) and the Thermal Infrared Sensor (TIRS). The OLI includes multispectral bands 1-7 and 9, operating at a spatial resolution of 30 meters. Additionally, the panchromatic band 8 operates at a higher resolution of 15 meters. TIRS bands 10 and 11 are initially collected at 100 meters but are resampled to 30 meters to align with the OLI multispectral bands during Level-1 product generation. The approximate scene size is 170 km north-south by 183 km east-west. The instruments on Landsat 9 are advanced versions of those found on Landsat 8. In this step, the satellite images provided critical information essential for estimating ETa using the ALARM model. Remote sensing software, including Arc/Info and ArcView GIS 10.8, was employed to process the satellite images and estimate the parameters required for the ALARM model.

2.4. Remote Sensing Data Collection

In this study, a series of satellite data from Landsat 8 and Landsat 9 was utilized, specifically from path 174 and row 38. The images, generated in 2024, were obtained from the United States Geological Survey (USGS) through their platform, http://earthexplorer.usgs.gov/. The Landsat 8 and 9 overpasses occurred at approximately 11:10 AM local time, featuring a spatial resolution of 30 meters and a spectral resolution of 12 bits. Although the data are available in 16 bits, allowing for pixel intensity values ranging from 0 to 65,535 gray levels, the 12-bit resolution enhances the detail of the information generated. Throughout the study period from February to May 2024, a total of six images were collected, with a combined revisit time of 8 days for the Landsat 8 and 9 satellites. Table 1 summarizes the key characteristics of these datasets.

2.4.1 Estimated Land Surface Temperature (LST)

The USGS provides the Top of Atmosphere Brightness Temperature (BT), which is calculated from Top of Atmosphere (TOA) radiance and two thermal constants, as detailed on https://landsat.usgs.gov/using-usgslandsat-8-product. The TOA radiance is captured by the TIRS, which operates using two spectral bands: Band 10 and Band 11. However, the USGS advises users to avoid relying on Band 11 data for quantitative analyses due to significant calibration uncertainties associated with this band. To calculate the LST from Landsat 8 and 9 satellite images, three bands are utilized: the fourth band (Red, with a wavelength of 0.64-0.67 micrometers), the fifth band (Near Infrared (NIR) with a wavelength of 0.85-0.88 micrometers), and the tenth band (TIRS1, with a wavelength range of 10.60-11.19 micrometers). In this study, data from Landsat 8 and 9 were accessed through the Earth Explorer website. The TIR Band 10 was utilized to estimate BT, while Bands 4 and 5 were employed to calculate the Normalized Difference Vegetation Index (NDVI). A total of six images from the Landsat 8 and 9 satellites were processed, with details of these images and the spectral bands used presented in Table 1. The estimation of LST involves several steps, utilizing thermal bands of Landsat 8 and 9. This process involves applying a series of equations via a raster image calculator, such as ArcMap or ArcGIS. The methodology is summarized as

a. Calculation of Top of Atmosphere (TOA) Spectral Radiance

The TOA spectral radiance is calculated using the equation (Allen et al., 2002):

$$TOA(L) = ML * Q_{cal} + AL$$
 (1)

Where ML = band-specific multiplicative rescaling factor from the metadata, Qcal = corresponds to band 10, and AL = band-specific additive rescaling factor from the metadata.

The specific equation for TOA can also be represented as (Allen et al., 2002):

$$TOA = 0.0003342 * B10 + 0.1$$
 (2)

The equation must be solved using the Raster Calculator tool in ArcMap.

b. Conversion of Radiance to Brightness Temperature (BT)

The TIRS band (B10) data should be converted from spectral radiance to BT using the thermal constants provided in the metadata (Allen et al., 2002):

$$BT = \left[\frac{\kappa_2}{\ln(\frac{\kappa_1}{T})} + 1 \right] - 273.15 \tag{3}$$

Where K1 and K2 = band-specific thermal conversion constants from the metadata, and L= TOA.

c. Calculation of Normalized Difference Vegetation Index (NDVI)

The NDVI is calculated using the NIR and RED band images according to the equation (Allen et al., 2002):

$$NDVI = \frac{NIR - RED}{NIR + RED} \tag{4}$$

Where NIR = reflectance of band 5, and RED = reflectance of band 4.

d. Calculation of Proportion of Vegetation (Pv)

The Pv is calculated according to (Allen et al., 2002):

$$Pv = \left(\frac{NDVI - NDVI\min}{NDVI\max - NDVI\min}\right)^2 \tag{5}$$

The minimum and maximum values of the NDVI image can be obtained from ArcGIS.

e. Calculation of Land Surface Emissivity (ε)

The ϵ is calculated as follows (Allen et al., 2002):

$$\varepsilon = 0.004 * Pv + 0.986$$
 (6)

The value of 0.986 corresponds to a correction factor of the equation.

f. Calculation of Land Surface Temperature (LST)

Finally, the LST is calculated using the equation (Allen et al., 2002):

$$LST = \frac{BT}{[1 + (0.00115 * \frac{BT}{1.4388}) * \ln(\varepsilon)]}$$
 (7)

By following these steps, the surface temperature map can be obtained, providing valuable information for the study's objectives.

2.4.2 Estimated Leaf Area Index (LAI)

The research the LAI can be estimated in the SEBAL model as a function of the Soil-Adjusted Vegetation Index (SAVI) (Bastiaanssen et al., 1998). An empirical relationship developed by Bastiaanssen et al. (1998) describes this relationship as follows:

$$SAVI = 0.69 - 0.59e^{-0.091*LAI} (8)$$

LAI represents the cumulative area of leaves per unit area of land at nadir orientation, providing a measure of vegetation density.

In the ALARM model, the method for estimating LAI is not explicitly defined. Therefore, LAI estimation in ALARM was conducted using Equation 8. The SAVI is calculated from Landsat 8 and 9 satellite images using the NIR and Red bands and is given by the formula (Bastiaanssen et al., 1998):

$$SAVI = \frac{(1+L)*(NIR-RED)}{(L+(NIR+RED))}$$
(9)

In this equation, L is the soil background correction factor, which varies between 0 and 1 depending on vegetation density. For this study, a value of L = 0.5 was assumed, as it has been shown to perform well under various vegetation conditions (Owaneh and Suleiman, 2018). By applying these equations, the LAI can be effectively estimated, contributing to the understanding of vegetation dynamics in the studied area.

2.4.3 Estimated Surface Albedo (α)

Surface albedo (α) is defined as the hemispherical surface reflectance of shortwave radiation across wavelengths of 0.3 to 3 µm. This dimensionless value ranges from zero to 1.0 and varies based on land cover type. Estimating α from Landsat 8 and 9 imageries typically requires starting from surface reflectance rather than digital numbers (dns). The input for albedo calculation must be a Landsat image that has been converted from DNs to TOA reflectance. Detailed formulas and explanations for this process can be found on the USGS site regarding the use of Landsat 8 products (Bastiaanssen et al., 1998). Surface reflectance is given by atmospheric correction procedures applied to the original land-sat images. We used the Yale method for estimating the albedo layer of the study area University Center for Earth Observation). https://yceo.yale.edu/how-convert-landsat-dns-albedo. The estimation method comes from the work of Liang et al. (2001) and the Yale Guide to Landsat 8 Image Processing at "Yale University/Understanding Landsat 8," https://surfaceheat.sites.yale.edu/understanding-landsat-8).

The estimation method is based on the work of who developed a series of algorithms for calculating albedo from various satellite images (Liang et al., 2001). The formula for converting Landsat 8 and 9 bands to albedo, as normalized by (Smith, 2010), is given by:

$$\alpha = \frac{(0.356*B2) + (0.130*B4) + (0.373*B5) + (0.058*B6) + (0.072*B7) - 0.0018}{1.016}$$
(10)

In this equation, B represents the Landsat bands 2, 4, 5, 6, and 7, with the note that Landsat band 3 (green) is not used in this calculation. This formula allows for the accurate estimation of surface albedo, contributing to the understanding of land surface properties in the study area.

3. Evapotranspiration (ET) Estimation Methods

3.1 Estimation Using the ALARM Model

To estimate ET using the ALARM model, we first identify the necessary mathematical relationships, including LAI, \mathcal{E} , α , LST, net radiation (Rn), soil heat flux (G), sensible heat flux (H), and latent heat flux (E λ). These parameters are crucial for calculating both instantaneous and daily ET. The method relies heavily on the energy balance between processes occurring at the Earth's surface and the atmosphere, known as the surface energy balance. This approach derives the latent heat flux, which is essential for estimating the daily ETa value through the energy balance equation, represented as (Bastiaanssen et al., 1998):

$$E\lambda = (Rn - G - H) \tag{11}$$

In this equation, Rn denotes net radiation (W/m^2), G represents soil heat flux (W/m^2), and H is the sensible heat flux (W/m^2). The latent heat flux E λ corresponds to the ET in terms of energy (W/m^2). The Rn is calculated as the difference between incoming and outgoing radiation, expressed by the formula (Bastiaanssen et al., 1998):

$$Rn = R_{S\downarrow} - \alpha R_{S\downarrow} + (1 - \varepsilon) * R_{L\downarrow}$$
(12)

Here, RS \downarrow is the incoming shortwave radiation (W/m²), RL \downarrow is the incoming long wave radiation (W/m²), α is the surface albedo, and ϵ is the surface emissivity. (For further information, have a look at (Allen et al., 2013). For soil heat flux G, this study employs equations developed by Bastiaanssen et al. (1998):

$$G: Rn = (Ts - 273.15)(0.0038 + 0.0074\alpha)(1 - 0.98 * NDVI^4)$$
(13)

Where Ts is the surface temperature in Kelvin.

To estimate ET using ALARM, the model converts surface canopy temperature (Ts) obtained from satellite data into aerodynamic temperature (Ti). This conversion corrects for the vegetation temperature profile, taking into account factors like LAI, canopy height, fractional cover, and leaf angle distribution. The aerodynamic temperature is then used to calculate heat flux based on Monin-Obukhov similarity theory (MOS). ET is

computed as a residual from the energy balance. ALARM uses different approaches to estimate H based on MOS, represented by the equation (Bastiaanssen, 2000):

$$H = \frac{(Ts - T\alpha) * Ku * \rho * C\rho}{\left\{ \ln\left(\frac{Za - do}{Zoh}\right) - \psi\left(\frac{Za - do}{L}\right)\right\}}$$
(14)

In this equation, Ta is the air temperature at height za in the surface sub layer, k is von Karman's constant (approximately 0.4), u* denotes friction velocity, ρ is air density, Cp is specific heat at constant pressure, z0h is the scalar roughness length for sensible heat, d0 is the displacement height, L is Obukhov length, and ψ is a stability correction function. Using Ts directly to estimate H is ineffective because the radiometric surface temperature estimated from satellite images differs from the aerodynamic temperature (Ti) needed for accurate calculations. ALARM addresses this by predicting Ti through corrections based on vegetation characteristics. To convert Ts to Ti, ALARM utilizes a rearranged form of the equation proposed by (Brutsaert and Sugita 1996):

$$Ts - Ta = \frac{H}{Ku * \rho * C\rho} \left[\ln \left(\frac{za - do}{zoh} \right) - \psi \alpha \right]$$
 (15)

In the study enhanced the ALARM model by introducing a dimensionless temperature dT (Suleiman and Crago, 2002). They defined the dimensionless temperature as (Ti – Ta)/(Tmax – Ta), where Ti is the aerodynamic temperature, Ta is the air temperature, and Tmax is the maximum surface temperature that would occur if all available energy (Rn – G) transformed into sensible H without any evaporation. Tmax is obtained by solving the previous equation for Ts, assuming H equals (Rn – G). Within ALARM, the relationship between H and dT is assumed to be linear (Brutsaert and Sugita, 1996):

$$H = (Rn - G) * dT \tag{16}$$

Based on equations (11) and (14), when (Ti - Ta) equals zero, dT will also be zero, resulting in H from equation (16) being zero. Conversely, when (Ti-Ta) equals (Tmax-Ta), dT equals one, leading H to equal (Rn-G). Using this assumption, ALARM estimates E in terms of dT (Brutsaert and Sugita, 1996):

$$E = (Rn - G)(1 - dT)$$
 (17)

For further details on ALARM and the dimensionless temperature, refer to the works of (Suleiman and Crago 2004; Suleiman and Al-Bakri, 2011; Owaneh and Suleiman, 2018). This study utilized six satellite images from Landsat 8 and 9, which revisit the same area every 16 days, to estimate ET using the ALARM model. The images were captured on the following dates: February 9, March 12, March 28, April 5, April 21, and May 15, 2024. From these images, key parameters such as α, NDVI, LAI, SAVI, LST, view angle (z), and time of satellite overpass (t) were either estimated or collected. Landsat 8 and 9 each feature 11 bands, with Band 10 being the thermal band used to estimate Ts. The multispectral bands (2, 3, 4, 5, 6, and 7) were employed to calculate NDVI, α, and LAI. The view angles and times of satellite overpass are documented in the metadata files accompanying each image. Additionally, canopy height—a crucial input for the ALARM model-was measured in the field on the same dates the images were captured. Figure 2 and Table 2 provide details on the number of days for which LST was available during the study period for the various pixels analyzed.

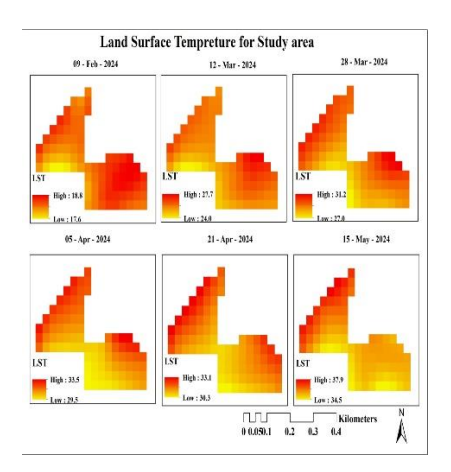


Figure 2: The minimum and maximum values of LST for the six image dates (Alqudah et al., 2024)

Table 2: Average estimated LST, LAI, NDVI, and α value for the six image dates.								
NO	Date	LST (2)	LAI	NDVI	SAVI	α		
1	9- FEB	18.17	0.502	0.211	0.316	0.166		
2	12-MAR	25.21	0.583	0.228	0.342	0.189		
3	28-MAR	28.85	0.718	0.254	0.382	0.221		
4	5- APR	31.25	0.851	0.273	0.41	0.23		
5	21- APR	31.77	0.767	0.263	0.395	0.237		
6	15-MAY	36.24	0.645	0.241	0.361	0.237		
Ave	rage	28.582	0.678	0.245	0.368	0.213		

The highest LST was recorded on May 15, 2024, with values of 37.35°C, 36.20°C, 35.87°C, and 35.01°C for the pixels P1, P2, P3, and P4, respectively. This peak corresponds to the warmest period in the study area. Conversely, the lowest temperatures were observed on February 9, 2024, with readings of 18.28°C, 18.32°C, 17.97°C, and 18.12°C in the same pixels, reflecting typical winter conditions. Figure 1 illustrates the minimum and maximum LST values throughout the study area based on Landsat 8 and 9 imageries collected on the specified dates. The measured albedo values ranged from 0.166 to 0.237, with an average of 0.22. The LAI values for the study area ranged from 0.502 to 0.851, averaging 0.678. To evaluate variability within the study area, LAI, NDVI, and SAVI were calculated for four pixels. The results, presented in Table 2, indicate significant variability in these indices, suggesting differences in soil conditions and crop management practices across the field.

3.2 Estimation Using the ETLook Model

The ETLook model estimates ETa by solving the P-M equation separately for vegetation and soil, allowing for the differentiation between transpiration (T) and evaporation (E). The equations for T and E are as follows (Bastiaanssen et al., 2012):

$$T = \frac{\Delta(Q_{canapy}^*) + \rho C \rho \frac{\Delta_e}{\gamma_{a,canapy}}}{\Delta + \gamma (1 + \frac{\gamma_{canapy}}{\gamma_{a,canapy}})}$$
(18)

$$E = \frac{\Delta(Q_{soil}^* - G) + \rho C \rho_{\overline{V_{Q,Soil}}}^{\Delta_e}}{\Delta + \gamma (1 + \frac{\overline{V_{soil}}}{V_{q,Soil}})}$$
(19)

Where $\Delta e =$ slope of the saturation vapor pressure curve (mbar/K), $\Delta =$ vapor pressure deficit (mbar), $\rho =$ air density (kg/m), Cp= specific heat of dry air (J/kg* K), $\gamma =$ psychrometric constant (mbar/K), G= soil heat flux (W/m), Q*canopy and Q*soil (W/m) = net radiation for canopy and soil, respectively, rcanopy and rsoil (s/m) = canopy and soil resistance, respectively; ra, canopy and ra, soil (s/m) = aerodynamic resistance for canopy and soil, respectively.

The ETLook model is implemented within the FAO Water Productivity (WaPOR) database, which serves as a portal for monitoring water productivity through open access to remotely sensed data. WaPOR provides access to a comprehensive water productivity database, allowing users to perform direct data queries, time series analyses, area statistics, and download key variables related to water and land productivity assessments. WaPOR datasets are accessible through dedicated FAO WaPOR APIs, which are being gradually published and documented. The database covers a period from 2009 to 2023 and is available at different spatial resolutions: continental scale (Level 1 at 250 m), country scale (Level 2 at 100 m), and project level (Level 3 at 30 m). The most recent version of WaPOR is WaPOR v3, and the methodology for compiling Eta data is based on the ETLook method as described by (Bastiaanssen et al., 2012). In this study, the finest resolution of WaPOR data utilized is 100 m (Level 2). The relevant datasets include layers for actual evaporation (E), transpiration (T), and actual evapotranspiration and interception (ETIa) at a decadal timescale (approximately every 10 days). ETIa represents the sum of soil evaporation (E), canopy transpiration (T), and interception (I)—the evaporation from rainfall intercepted by leaves. Each pixel value corresponds to the average daily ETIa during a given dekad. An overview of the WaPOR data used in the analyses is presented in Table 3.

Table 3: The WaPOR layers used for the analyses.						
WaPOR data Layer	Spatial Resolution	Temporal Resolution				
Evaporation (E) in mm/day	100 m	Dekadally (approximately every 10 days)				
Transpiration (T) in mm/day	100 m	Dekadally (approximately every 10 days)				
ETa and Interception (Dekadal)	100 m	Dekadally (approximately every 10 days)				

The calculation of ETIa is based on the ETLook model described in Bastiaanssen et al. (Bastiaanssen et al., 2012), with base input layers, including NDVI and albedo, derived from the Proba-V satellite.

3.3 Validation of ET Estimates

To validate the different ET results obtained in this study, various ere employed, including mean, range, statistical parameters w coefficient of variation, standard deviation, and root mean square error (RMSE). The details of these statistical methods can be found in any standard statistics book. The ETa produced by Landsat 8/9 using the ALARM model was compared with estimates derived from the ETLook model, enabling a comprehensive evaluation of both methods. The validation process involved calculating RMSE between the ALARM and ETLook methods. Microsoft Excel 2010 was utilized for all statistical analyses and data chart generation. The primary objectives of the statistical analyses included testing the performance of the ALARM model, and evaluating the accuracy of the ETLook model. These analyses provide a thorough assessment of the accuracy and reliability of the various ET estimation methods applied in this study, highlighting the strengths and weaknesses of both the ALARM and ETLook models in estimating ETa for date palm cultivation.

4. RESULTS AND DISCUSSIONS

4.1 Estimated Dairy ETa by ALARM Model

Figure 3 illustrates the temporal dynamics of estimated ETa values derived from the ALARM model for four distinct pixels (p1, p2, p3, and p4) within the study area over the period spanning from February 9 to May 15.



Figure 3: ALARM ETa values for four pixels.

As shown in Figure 3, the data reveals a clear and consistent upward trend in ETa across all four pixels throughout the monitored timeframe. Starting from relatively lower values in early February, the ETa estimates steadily increased, reaching their peak levels by mid-May. This consistent increase in ETa aligns with the progression of the growing season for the date palms, as the plants' water consumption requirements climbed in tandem with their growth and development. This behavior could be mainly attributed to the temporal variations of LST in the study area (Figure 4), where the curve of LST had the same trend.

While the overall temporal trajectory was analogous for the four pixels, there were noticeable differences in the absolute ETa magnitudes recorded for each individual location. The four pixels can be broadly categorized into two groups: p1 and p2 exhibited relatively lower ETa values compared to the higher estimates observed for p3 and p4. This spatial heterogeneity in ETa suggests that there are localized factors within the study area, such as soil characteristics, microclimate, or management practices, that are

influencing the evapotranspiration dynamics in a differentiated manner across the monitored locations.

The range of estimated daily ETa values spanned from around 2.5–3 mm/day in early February to 5-5.5 mm/day by mid-May, underscoring the significant increase in water consumption by the date palms as the growing season progressed. Figure 4 provided offers valuable insights into the temporal variations in LST within the study area, as estimated from Landsat satellite imagery over the monitoring period from January 29 to May 28.

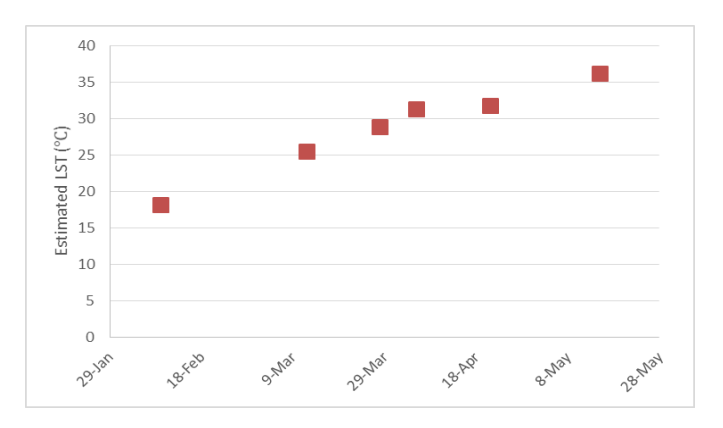


Figure 4: Variations of LST estimated from Landsat images at the study area.

The data presented in Figure 4 reveals a clear and pronounced upward trend in LST values throughout the study period. The surface temperature in the study area steadily increased as the growing season progressed, rising from around 15°C in late January/early February to nearly 35°C by the end of May—a substantial increase of approximately 20°C. This substantial warming of the land surface over the five-month timeframe reflects the significant seasonal changes in the climatic conditions of the study region.

While the overall trend is decidedly upward, the LST values do exhibit some fluctuations from one observation date to the next. For instance. there are more pronounced increases in LST between the January 29 and February 18 measurements, as well as between the March 9 and March 23 data points, followed by relatively smaller changes in the subsequent periods. These short-term fluctuations suggest that in addition to the broader seasonal patterns, other dynamic factors, such as weather patterns or localized meteorological conditions, are influencing the surface temperature within the study area over shorter timescales. The sensitivity of LST to the seasonal progression is particularly noteworthy, as the temperature rises in close alignment with the advancing growing season. This strong correlation between LST and the seasonal cycle is an important consideration when analyzing the ET dynamics of the date palm crop, as presented in Figure 3. The increasing surface temperatures likely play a significant role in driving the observed upward trend in estimated ETa over the course of the monitoring period.

The estimated daily ETa of date trees from the ALARM model ranged from 2.58 mm/day on February 9 to 5.23 mm/day on May 15 (Figure 3). The increasing surface temperatures, as shown in Figure 6, likely drive the observed upward trend in estimated evapotranspiration, underscoring the significance of understanding the interrelationships between climatic factors and crop water consumption patterns for effective water management strategies in date palm cultivation. For crop ET estimation, the growing season is divided into four stages: initial, development, mid, and late stages. For vegetables, the initial stage starts at planting and ends when the ground cover is around 10%; the development stage begins immediately after the initial stage and continues until the ground cover reaches around 85–90%. The date trees were in mid-stage during the study period. During the mid-stage, the Palm Date Kc value is 0.95.

Daily ETa was estimated from Landsat image data for four pixels in the study area. The mean daily ALARM ETa estimates were 2.58, 3.66, 4.32, 4.65, 4.94, and 5.23 mm/day on February 9, March 12, March 28, April 5, April 21, and May 15, respectively (Figure 3). Generally, it was noticed that the estimates were higher than ALARM ETa values. The detailed comparisons at specific dates provide further insights. On February 9, the ALARM ETa was 2.582 mm/day. On March 12, the ALARM ETa was 3.657 mm/day. Similar discrepancies are observed across the other observation dates, reinforcing the tendency of the ALARM model to underestimate the crop's water consumption requirements. To assess the ALARM ETa

variations within the study area, the LAI and LST were computed from the

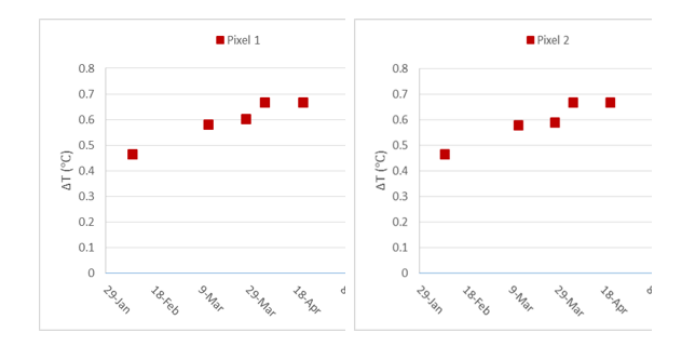
satellite images for four pixels, as shown in Tables 4.

	Table 4: Summary statistics of LAI, LST, and ALARM ETa values estimated by Landsat images for different pixels.											
LAI				LST			ALARM ETa					
Pixel ID.	Min	Max	Mean	Σ	Min	Max	Mean	σ	Min	Max	Mean	σ
P1	0.54	0.68	0.62	0.05	18.28	37.65	30.54	6.78	2.55	5.02	3.99	1.03
P2	0.46	0.71	0.61	0.08	18.32	36.39	30.03	6.33	2.54	5.18	4.09	1.11
Р3	2.06	6.60	0.65	0.11	17.97	35.56	29.41	6.29	2.65	5.26	4.34	0.93
P4	2.06	6.60	0.82	0.28	18.11	35.35	28.83	5.99	2.59	5.45	4.48	0.98

The spatial analysis of the biophysical parameters presented in Table 4 reveals notable variations within the study area, which have important implications for understanding the ET dynamics of the date palm crop. The LAI values ranged from 0.54 to 0.68, with a mean of 0.62 and a σ of 0.05. This moderate variability in the vegetation cover across the different pixels suggests heterogeneity in the crop growth and canopy development within the study area. In contrast, the LST exhibited a much wider range, fluctuating from 18.28°C to 36.39°C, with a mean of 30.54°C and a σ of 6.78°C. This substantial variation in the thermal characteristics of the land surface across the pixels highlights the spatial complexity of the microclimate within the cultivated area.

The ALARM model's estimated ETa values also showed considerable variability, ranging from 3.99 mm/day to 4.48 mm/day, with a mean of 4.20 mm/day and a σ of 0.98 mm/day. This spatial heterogeneity in the ETa estimates is likely influenced by the observed differences in the biophysical parameters, particularly the LAI and LST. The higher LAI values observed in the study area (up to 0.85) suggest that the increased vegetation cover played a role in enhancing the energy available for the evapotranspiration process, contributing to the relatively higher ALARM ETa estimates. Furthermore, the substantial variations in LST across the pixels suggest that the thermal environment is a significant factor influencing the ET dynamics within the study area. The higher surface temperatures are expected to increase the atmospheric demand for water, thereby driving higher ET rates. The interplay between the LAI and LST likely contributed to the observed variability in the ALARM ETa estimates across the different pixels. As shown in Table 4, there was a difference between the mean estimated LAI for Landsat pixels. It was found LAI ranged between 0.60 and 0.85 and for Landsat pixels. The LST ranged between 28.83°C and 30.54 °C for Landsat pixels. Table 4 shows ALARM ET based on estimated LAI. In ALARM, by increasing LAI, the aerodynamic temperature Ti decreases. Thus, the value of H decreases, and more energy is available for ET. It was found that the main factor for high ALARM ETa obtained from Landsat data was mainly high LAI.

Most farms in Jordan are relatively small (around three ha), and the use of Landsat 8 satellite images to estimate ET for an individual farm may not provide an accurate representation of the actual ET, as some pixels may be "mixed pixels" containing the target crop (date palm) as well as other elements, such as bare soil, other crops, and buildings. In this study, four full-crop pixels (containing only date palms) were selected from the middle of the date palm field to minimize the influence of these mixed pixels. Results in Figure 5 showed that dimensionless temperature (ΔT) values for the different pixels during the study period. The ΔT values were greater than zero for all pixels. Within the same pixel, the variation between maximum ΔT and minimum ΔT was not high during the study period. The ΔT values ranged from (0.57) for pixel P4 to (0.6) for pixel P1. For ideally, ΔT ranges from 0 when ET is maximum (ETmax = Rn-G) to 1 when ET is minimum (ETmin = 0). A low value of ΔT indicates sufficient soil moisture while high values of ΔT indicate limited soil moisture, available to meet ET demands.



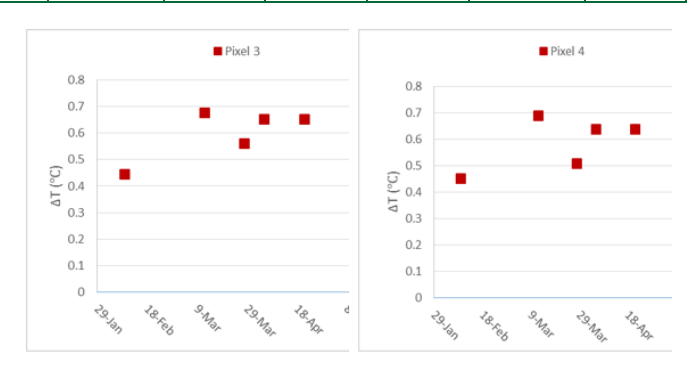


Figure 5: Dimensionless temperature (ΔT) for the different pixels for the study period.

The present study is highly consistent with some previous research. estimated water requirements for a mixture of olive and date trees using daily MODIS satellite images and the ALARM model (Derdar, 2011). The RMSE between ALARM and measured daily ET was 0.65 mm/day. Study of to estimate the optimal water requirements for date palm trees in Al-Hassa Oasis (Biro et al., 2020). Landsat 8 satellite data was used to estimate the daily, monthly, and yearly evapotranspiration rates of the trees by using the SEBAL model. The results showed a significant agreement level between the SEBAL model and the FAO P-M method with an RMSE of 0.84 mm/day. The analysis estimated the ET of alfalfa crops using the ALARM method and compared it with measured alfalfa ET computed from a water balance equation (Suleiman and Al-Bakri, 2011). The results showed RMSE for ALARM estimates of alfalfa was 0.87 mm/day.

4.2 Comparative Analysis of ETLook ETa from the FAO WaPOR Portal

The ETLook-WaPOR approach partitions the WaPOR ETa to evaporation and transpiration using the modified PM equation, which differentiates the net available radiation and resistance formulas based on the vegetation cover according to the ETLook model. Daily ETLook ETa was estimated from the Wapor portal database for the different pixels in the study area and is presented in Figure 6.



Figure 6: ETLook Dekadal ETa values for the different pixels.

Wapor portal ETLook ETa data represent Dekadal (10-day) composites of ET, which contain the average daily ET during the Dekadal period. At national scale 100 m resolution (called Level 2), the Wapor ETa data set was acquired using observations from MODIS and PROBA-V satellite thermal data. Figure 6 shows a clear increasing trend in the ETa values over the study period, starting from around 0.5 mm/day in early February and reaching a maximum of approximately 2.5 mm/day during the Dekadal period from 1-10 April, after which the values began to decrease. This temporal pattern reflects the changing environmental conditions and

increasing crop water demand as the growing season progresses. When examining the differences between the pixels, the data reveals significant spatial variability in the ETa values. For instance, during the 1-10 February Dekadal period, the ETa ranged from around 0.5 mm/day for P1 to over 1.0 mm/day for P4. By the 1-10 May Dekadal period, this range had expanded, with P1 recording an ETa of around 1.2 mm/day, while P4 reached nearly 2.5 mm/day. This spatial heterogeneity in ET suggests the influence of site-specific factors, such as soil moisture, vegetation cover, and microclimate conditions, on the crop water use within the study area. To evaluate the performance of the ETLook model, in order to check whether it overestimates or underestimates ETa in comparison to the FAO56 method, compare the average daily values of Wapor ETa, derived from the average daily values of each Dekadal period (10-days).

4.3 Comparative Analysis of ET Estimation: ALARM Vs. ETLook

The estimation of ETa for date palm cultivation was carried out using two distinct methodologies: the ALARM model and the ETLook algorithm. Each approach offers unique insights into the water requirements of date palms and highlights the spatial variability of ETa across the study area. The ALARM model employs an energy balance approach, integrating biophysical parameters such as LAI and LST derived from Landsat satellite

imagery (Asadi and Karami, 2020). This model is particularly adept at capturing the complexities of ET dynamics across various locations due to its sensitivity to changes in these parameters. By relying on high-resolution satellite data, the ALARM model can effectively account for variations in canopy structure and thermal conditions, which are critical for understanding the water needs of date palms throughout their growing season (Asadi and Karami, 2020).

In contrast, the ETLook algorithm utilizes a modified Penman-Monteith equation to partition ETa into evaporation and transpiration components based on vegetation cover. This method leverages data from the WaPOR portal and produces Dekadal (10-day) composites of ETa, which smooth out daily fluctuations to provide a more generalized view of water consumption (Sejine and Anane, 2024). By offering three readings per month for each pixel, the ETLook algorithm allows for a broader assessment of ET trends but may not capture the finer details of localized conditions as effectively as the ALARM model. The results from both models reveal significant insights into the water requirements of date palms. Table 5 summarizes the estimated ETa values for date palm cultivation, comparing the ALARM model and the ETLook algorithm across four different pixels. This data includes minimum, maximum, mean, and standard deviation values for each method, as well as the root mean square error (RMSE) for each pixel.

Table 5: Summary statistics of ETa estimated by ALARM and ETLook for different pixels.									
			ALA	RM ETa			ETLo	ok ETa	
Pixel ID.	RMSE	Min	Max	Mean	σ	Min	Max	Mean	σ
P1	2.861432	2.5467	5.02	3.996	1.026	0.9	1.9	1.35	0.497
P2	2.991861	2.5417	5.18	4.092	1.108	0.9	1.8	1.3	0.3795
Р3	2.484986	2.6489	5.26	4.3433	0.9273	0.9	2.3	1.9	0.5329
P4	2.458642	2.5923	5.45	4.4855	0.9788	1.2	2.5	2.083	0.475
Average	2.6992302	2.5824	5.23	4.23		0.975	2.125	1.66	

The analysis presented in Table 5 highlights significant disparities between the ALARM model and the ETLook algorithm in estimating ETa for date palm cultivation. The ALARM model consistently yields higher ETa values across all pixels, with mean values reaching up to 4.4855 mm/day for pixel P4, while the ETLook algorithm peaks at a mean of only 2.083 mm/day. This discrepancy indicates that the ALARM model is more sensitive to biophysical parameters and environmental conditions, effectively capturing a broader range of water requirements essential for optimal growth.

When examining the minimum daily ETa values, it reveals that the ETLook algorithm consistently produces lower estimates than the ALARM model across all pixels. For instance, the minimum daily ETLook value for pixel P1 is 0.9 mm/day, whereas the ALARM model's minimum is 2.5467 mm/day, resulting in a relative difference of approximately 64.7%. This pattern persists across pixels, with relative differences ranging from 64.7% in pixel P1 to about 61.5% in pixel P4, where the minimum ETLook value is 1.2 mm/day compared to the ALARM model's 2.5923 mm/day. Similarly, the maximum daily ETa values for the ETLook algorithm fall below those of the ALARM model. For example, the maximum ETLook value for pixel P1 is 1.9 mm/day, while the ALARM model's maximum is 5.02 mm/day, showing a relative difference of about 62.2%. This trend continues across all pixels, with maximum relative differences reaching 60.5% in pixel P4, where the maximum ETLook value is 2.5 mm/day compared to the ALARM model's 5.45 mm/day.

In terms of variability, the σ for the ALARM model ranges from 0.9273 mm/day to 1.108 mm/day, indicating greater variability in its estimates. In contrast, the ETLook shows lower σ , ranging from 0.3795 mm/day to 0.5329 mm/day. The analysis of ETa values from both the ALARM model and the ETLook reveals a range of RMSE values between 2.458 mm/day and 2.992 mm/day, with an average RMSE of approximately 2.7 mm/day. This RMSE range indicates the degree of deviation of the estimated ETa values from the observed measurements, highlighting the overall accuracy of both models in estimating ET for date palm cultivation. The average RMSE suggests that, while both models provide valuable insights, there is variability in their performance across different pixels, emphasizing the importance of context-specific factors in ET estimation.

This analysis emphasizes the need to carefully select ET estimation methodologies based on specific agricultural contexts. In heterogeneous landscapes like those used for date palm cultivation, combining the strengths of both models can improve water use efficiency and inform sustainable agricultural practices. Ultimately, accurate ETa estimation is crucial for effective water resource management in arid and semi-arid regions. Table 6 provides a comprehensive comparison between the ALARM model and the ETLook algorithm based on their methodologies, data sources, performance, and results in estimating ETa for date palm cultivation.

Table 6: Comparison of ALARM and ETLook models for ETa estimation in agriculture.						
Criteria	ALARM Model	ETLook Algorithm				
Methodology	Utilizes an energy balance approach that incorporates LAI and LST derived from Landsat satellite imagery. This model calculates ETa based on the available energy for ET processes.	Employs a modified Penman-Monteith equation to separate evaporation and transpiration based on vegetation cover. This algorithm uses thermal data from the WaPOR portal to estimate ETa.				
Utilizes Landsat 8 and 9 satellite imagery, prov resolution data (30 m). This allows for detailed localized conditions affecting ETa.		Relies on the WaPOR portal, which uses data from MODIS and PROBA-V satellites at a national scale with a resolution of 100 m.				
Spatial Resolution	High spatial resolution (30 m) enables precise estimation of ETa across various microenvironments within the study area.	National scale, 100 m resolution, which may lead to less detail in heterogeneous landscapes.				

Table	Table 6 (Cont.): Comparison of ALARM and ETLook models for ETa estimation in agriculture.							
Temporal Resolution	Provides daily ETa estimates, allowing for detailed monitoring of temporal changes in crop water requirements.	Offers Dekadal (10-day) composites of ETa, which smooths out daily variations but may miss critical fluctuations in water demand.						
ETa Range	Estimates range from 2.5824 mm/day to 5.23 mm/day, reflecting the increasing water demands of date palms during the growing season.	Estimates range from approximately 0.975 mm/day to 2.125 mm/day, indicating a more conservative water use estimation.						
Trend in ETa	Displays a consistent upward trend throughout the growing season, aligned with the physiological needs of the date palms.	Shows an increasing trend but at lower values overall, which may not fully capture the peak water demands of the crop.						
Spatial Variability	Exhibits notable differences in ETa across various pixels, influenced by localized factors such as soil moisture, crop management practices, and microclimates.	Shows significant spatial variability; however, the broader scale may obscure finer details of localized conditions.						
Strengths	Highly sensitive to changes in biophysical parameters, effectively reflecting the complexities of ET dynamics across different environments. Ideal for detailed localized assessments.	Useful for broader regional evaluations, providing a simpler methodology that can be easier to implement in large-scale assessments.						
Weaknesses	Risk of overestimating ETa if not properly calibrated; requires accurate input data for optimal performance.	Tends to underestimate ETa during peak demand periods, potentially leading to insufficient irrigation recommendations.						
Performance Metrics	Generally provides higher ETa estimates compared to the ETLook algorithm, demonstrating greater responsiveness to variations in LAI and LST.	Produces lower estimates of ETa, which may indicate a conservative approach that does not fully account for localized water needs.						

Overall, while both methods provide valuable insights into ETa for date palm cultivation, the ALARM model appears better suited for detailed assessments due to its responsiveness to changing biophysical parameters. The ETLook model, while useful for broader regional evaluations, may underestimate the water requirements of date palms, particularly during peak growth periods. Understanding these differences is crucial for optimizing irrigation strategies and enhancing water management practices in date palm cultivation. This analysis underscores the importance of selecting the appropriate method based on the specific agricultural context and the desired level of detail in water management

strategies, ultimately contributing to improved water use efficiency and sustainability in date palm cultivation.

4.4 Comparative Analysis of Current Study and Previous Research

Table 7 summarizes the methodologies, results, and focuses of the current study on date palm ET in Jordan, specifically utilizing the ALARM and ETLook models, alongside several relevant studies from the literature. This comparison highlights key differences and similarities in approaches and findings.

Table 7: Summary of studies on ETa and crop water management.							
Study	Method Used	Results	Focus				
Current Study	ALARM model and ETLook model, Landsat 8 & 9 satellite imagery.	ALARM ETa values: 2.5824-5.23 mm/day; average 4.23 mm/day. ETLook values: 0.975-2.125 mm/day; average 1.66 mm/day.	Estimation of ETa in date palms.				
(Sejine and Anane, 2024)	(Sejine and Anane, 2024) WetSpass-S model and FAO ETLook model, Sentinel-2 imagery. ETa values for 2020/2021: 350 mm/year; WetSpass-S generally provided higher values than FAO for surface water; significant differences over 800 mm in irrigated areas.		Assessment of ETa and water balance components in Grombalia phreatic aquifer.				
(Wu et al., 2022)	Multiscale network with coordinate convolutional and attention modules.	Accuracy scores: OA 0.9481, kappa 0.9115; improves mapping accuracy by addressing spectral and spatial challenges.	Crop mapping using remote sensing technology.				
(Degerli and Çetin, 2022)	RS-GIS technology, MLC algorithm, MLP-ANN for future predictions.	MLP-ANN accuracy: 72%; predicted land use changes for 2030 with significant shifts in land cover.	Land use/cover analysis using remote sensing.				
(Al-Bakri et al., 2022)	Remote sensing, GIS, climatic data, WaPOR data.	Highlighted importance of WaPOR for AWA; identified underestimation of percolated water.	Agricultural water accounting in Jordan Valley				
(Asadi and Karami, 2020)	Analysis of Landsat 7 & 8 images, SEBAL, METRIC, and ALARM methods.	ALARM showed ET rates but less accuracy compared to SEBAL; highest ET on July 1, 2018 (7.86 mm/day).	ET measurement in wheat crops.				
(Blatchford et al., 2020)	Assessment of irrigation performance indicators at varying resolutions.	Different resolutions affected adequacy, equity, and productivity; higher resolutions captured more variability.	Irrigation performance assessment.				
(Kalua et al., 2020)	Comparison of sUAS and EOS data for ET measurement.	sUAS ET estimates lower than EOS by >0.5 mm; useful for local irrigation management.	Evaluating ET using sUAS and earth observation.				
(Trottier et al., 2020)	Geospatial analysis and qualitative methods.	Highlighted social implications of date palm cultivation on labor and land tenure.	Socioeconomic impacts of agricultural transformation.				

Table 7(Cont.): Summary of studies on ETa and crop water management.							
(Tan et al., 2018)	(Tan et al., 2018) Satellite imagery and empirical downscaling.		Water management through ET monitoring.				
(Van et al., 2017)	ALOS/AVNIR-2 and Landsat/OLI&TIR sensors, Maximum Likelihood Classification.	Significant reduction of urban green space from 2007-2017; projected decline in vegetation cover.	Assessment of urban green space and sustainability in Nha Trang.				
(Owaneh and Suleiman, 2018)	ALARM and SEBAL models, Landsat 8 imagery, lysimeter data.	Modified ALARM provided more accurate ET estimates than SEBAL; both models underestimated ET.	Testing ALARM and SEBAL against lysimeter data.				
(Al Zayed et al., 2016)	Remote sensing methods (SSEB, MODIS, and NDVI).	SSEB and MOD16A2 were most suitable for estimating ETa; effective for regional and daily scale.	Evaluation of RS methods for ETa in irrigation schemes in Sudan.				
(Al-Antary et al., 2014)	Field surveys and classification of insect pests.	Identification of various arthropod pests affecting date palms; created identification keys.	Insect pest survey and classification in date palms.				
(Sperling et al., 2014)	Modified Jarvis-Penman-Monteith model incorporating water salinity.	High water salinity reduced palm tree ET; developed a model for irrigation recommendations; 20% water reduction.	Impact of water quality on palm tree ET.				
(Ghamarnia et al., 2014)	Drainable lysimeter and Penman- Monteith method.	Water requirement for black cumin: 724 mm; established crop coefficients and regression models for ET.	Water requirements and crop coefficients for medicinal plants.				
(Bastiaanssen et al., 2012)	ETLook model, optical and passive microwave sensors.	ET: 1.2 mm/day; basin-wide ET: 496 ± 16.8 km ³ /yr; average net radiation: 112 W/m ² .	Surface energy fluxes and ET in the Indus basin.				
(Suleiman and Al-Bakri, 2011)	Water balance equation for ET measurement in alfalfa.	ET rates: 6-10 mm/day; RMSE for ALARM: 0.87 mm/day; ALARM ET closely aligned with FAO-56.	ET in irrigated alfalfa.				
(Derdar, 2011)	MODIS satellite images and eddy covariance system.	Average ET: 5.67 mm/day (measured), 5.61 mm/day (ALARM); RMSE: 0.65 mm/day.	ET estimation for olive and date trees.				
(Suleiman et al., 2008)	ALARM method across different ecological zones.	Significant variability in wheat ET is influenced by soil types, vegetation, and irrigation practices.	ET of wheat in Jordan.				

The comparative analysis reveals distinct methodologies and results across the various studies. The current study utilizes the ALARM and ETLook models, integrated with high-resolution Landsat 8 and 9 imageries, to estimate ETa specifically for date palms. This approach yielded ETa values between 2.58 mm/day and 5.23 mm/day, with an average of 4.23 mm/day for the ALARM model, while the ETLook model provided lower estimates ranging from 0.975 mm/day to 2.125 mm/day. This significant disparity in results underscores the critical role of model selection based on the specific agricultural context.

According to analysis, employed the WetSpass-S model and FAO ETLook model using Sentinel-2 imagery, reporting an annual ETa of 350 mm/year (Sejine and Anane, 2024). Their findings highlight the limitations of utilizing surface water models without considering crop-specific dynamics. Similarly, applied a multiscale network for crop mapping, achieving high accuracy scores (OA 0.9481, kappa 0.9115) but did not focus on ETa specific to date palm (Wu et al., 2022). Although these studies address various agricultural issues, such as water balance and land use changes, they do not delve into the specificities of ETa in date palms. The focus on date palms in the current study allows for tailored insights that are particularly relevant to regions reliant on this crop, enhancing practical applicability.

Another noteworthy comparison is with who utilized remote sensing and machine learning techniques for land use analysis (Degerli and Çetin, 2022). While their study achieved a prediction accuracy of 72%, it lacked the detailed ETa estimation provided in our research. Furthermore, analyzed ET rates in wheat crops using SEBAL and ALARM methods, noting that ALARM showed less accuracy compared to SEBAL, which emphasizes the need for tailored methodologies depending on the crop type and environmental conditions (Asadi and Karami, 2020).

The current study's focused methodology on date palms distinguishes it from broader studies that often address multiple crops or agricultural systems. This specificity is crucial, as it allows for targeted irrigation strategies that enhance water use efficiency. The results from this study align with findings from which emphasize the importance of effective water management techniques and the suitability of remote sensing

methods for ETa estimation .The study tested the ALARM model against lysimeter data, finding it slightly more accurate than SEBAL, which supports the current study's methodology (Owaneh and Suleiman, 2018). Other studies, like those further contextualize the significance of ET estimation and water quality in agricultural practices (Al Zayed et al., 2016; Sperling et al., 2014).

Overall, these studies demonstrate the diversity of methodologies in remote sensing applications, underscoring their relevance in both agricultural and urban contexts. The integration of findings from these various studies not only enhances understanding of water requirements and management strategies for date palms in Jordan but also informs broader discussions on sustainability and resource management in arid regions. This comprehensive perspective is essential for improving agricultural productivity and environmental resilience in the face of climate challenges.

5. CONCLUSION

This study offers a comprehensive evaluation of the water requirements for date palm cultivation in Jordan, focusing on the importance of accurately estimating ETa to support sustainable agricultural practices. Through a detailed comparative analysis of the Analytical ALARM model and the ETLook model, we have highlighted significant differences in their performance and applicability. Conducted from February 9 to May 15, 2024, this research utilized six satellite images from Landsat 8 and 9, yielding crucial insights into the water dynamics of date palm. The ALARM model demonstrated a range of ETa values from 2.58 mm/day. In contrast, the ETLook model provided lower estimates, from 0.975 mm/day to 2.125 mm/day. This disparity indicates that while the ALARM model is capable of capturing the higher water demands during critical growth phases, the ETLook model may not fully reflect the irrigation needs during these periods.

The findings also revealed a notable spatial variability in ETa estimates, with the ALARM model effectively representing diverse canopy structures,

as evidenced by its LAI values ranging from 0.54 to 0.68. Additionally, LST readings exhibited a significant correlation with ETa, ranging from 18.28°C to 36.39°C, highlighting the importance of thermal conditions in evapotranspiration processes. Given these insights, we propose that integrating both models—leveraging the ALARM model's strengths for localized assessments and the ETLook model's broader regional applicability—can enhance irrigation management strategies. This dual approach not only improves water use efficiency but also promotes sustainable agricultural practices tailored to the specific needs of date palm orchards in Jordan.

As we face increasing climate variability and water scarcity, the strategies developed from this study are vital for ensuring the resilience of agriculture in arid and semi-arid regions. By synthesizing our findings with existing literature, we provide a robust framework for future research and practical applications in agricultural water management. This comprehensive understanding of ETa estimation is crucial for optimizing irrigation practices and advancing the sustainability of agricultural systems in Jordan and similar environments.

REFERENCES

- Acharya, B.S., Bhandari, M., Bandini, F., Pizarro, A., Perks, M., Joshi, D.R., Wang, S., Dogwiler, T., Ray, R.L., Kharel, G., and Sharma, S., 2021. Unmanned Aerial Vehicles in Hydrology and Water Management: Applications, Challenges, and Perspectives. Water Resour. Res. 57. https://doi.org/10.1029/2021WR029925
- Al Zayed, I.S., Elagib, N.A., Ribbe, L., Heinrich, J., 2016. Satellite-based evapotranspiration over Gezira Irrigation Scheme, Sudan: A comparative study. Agric. Water Manag. 177, Pp. 66–76. https://doi.org/10.1016/j.agwat.2016.06.027
- Al-Antary, T.M., Al- khawaldeh, M.M., Ateyyat, M.A., 2014. Keys for identification arthropods pests attacking date palm. Bothalia Journa 44, Pp. 60–71.
- Al-Bakri, J.T., D'Urso, G., Batchelor, C., Abukhalaf, M., Alobeiaat, A., Al-Khreisat, A., Vallee, D., 2022. Remote Sensing-Based Agricultural Water Accounting for the North Jordan Valley. Water 14, 1198. https://doi.org/10.3390/w14081198
- Al-Khayri, J.M., Naik, P.M., 2017. Date palm micropropagation: Advances and applications. Ciência e Agrotecnologia 41, Pp. 347–358. https://doi.org/10.15 90/1413-70542017414000217
- Allen, A.P., Brown, J.H., Gillooly, J.F., 2002. Global Biodiversity, Biochemical Kinetics, and the Energetic-Equivalence Rule. Science (80). 297, Pp. 1545–1548. https://doi.org/10.1126/science.1072380
- Allen, R.J., Norris, J.R., Wild, M., 2013. Evaluation of multidecadal variability in CMIP5 surface solar radiation and inferred underestimation of aerosol direct effects over Europe, China, Japan, and India. J. Geophys. Res. Atmos. 118, Pp. 6311–6336. https://doi.org/10.1002/jgrd.50426
- Alqudah, S., Suleiman, A., Aljaafreh, S., 2024. Estimation Of Daily Actual Evapotranspiration For Dates Using The Alarm. J. Southwest Jiaotong Univ. 59. https://doi.org/10.35741/issn.0258-2724.59.3.35
- Asadi, M., Karami, M., 2020. Estimation of Evapotranspiration in Fars Province Using Experimental Indicators. J. Appl. Res. Geogr. Sci. 20, Pp. 159–175. https://doi.org/10.29252/jgs.20.56.159
- Atasever, U.H., Ozkan, C., 2018. A New SEBAL Approach Modified with Backtracking Search Algorithm for Actual Evapotranspiration Mapping and On-Site Application. J. Indian Soc. Remote Sens. 46, Pp. 1213–1222. https://doi.org/10.1007/s12524-018-0816-9
- Ayasrah, S., Hanandeh, A., 2024. Bassmati Community: Innovating WASH and Climate Solutions in Jordan. Int. J. Sustain. Dev. Plan. 19, Pp. 347–354. https://doi.Org/10.18280/ijsdp.190133
- Ayman Suleiman, J.A.-B., 2011. Estimating actual evapotranspiration using ALARM and the dimensionless temperature. Evapotranspiration. . Croatia.
- Ayyad, S., Al Zayed, I.S., Ha, V.T.T., Ribbe, L., 2019. The Performance of Satellite-Based Actual Evapotranspiration Products and the Assessment of Irrigation Efficiency in Egypt. Water 11, 1913. https://doi.org/10.3390/w11091913
- Bani Ataa, S., Jamrah, A., Al-Zghoul, T.M., 2024. Environmental Impact Of Wastewater Treatment Plant Using Lifecycle Assessment – Case Study In Jordan. Water Conserv. Manag. 8, Pp. 480–486. https://doi.org/ http://doi.org/10.26480/wcm.04.2024.480.486

- Bastiaanssen, W.G.., 2000. SEBAL-based sensible and latent heat fluxes in the irrigated Gediz Basin, Turkey. J. Hydrol. 229, Pp. 87–100. https://doi.org/10.1016/S0022-1694(99)00202-4
- Bastiaanssen, W.G.M., Cheema, M.J.M., Immerzeel, W.W., Miltenburg, I.J., Pelgrum, H., 2012. Surface energy balance and actual evapotranspiration of the transboundary Indus Basin estimated from satellite measurements and the ETLook model. Water Resour. Res. 48. https://doi.org/10.1029/2011WR0 10482
- Bastiaanssen, W.G.M., Pelgrum, H., Wang, J., Ma, Y., Moreno, J.F., Roerink, G.J., van der Wal, T., 1998. A remote sensing surface energy balance algorithm for land (SEBAL). J. Hydrol. Pp. 212–213, 213–229. https://doi.org/10.1016/S0022-1694(98)00254-6
- Biro, K., Zeineldin, F., Al-Hajhoj, M. R., Dinar, H.A., 2020. Estimating irrigation water use for date palm using remote sensing over an oasis in Arid region. . Iraqi J. Agric. Sci. 51, Pp. 1173–1187.
- Blatchford, M., M. Mannaerts, C., Zeng, Y., Nouri, H., Karimi, P., 2020. Influence of Spatial Resolution on Remote Sensing-Based Irrigation Performance Assessment Using WaPOR Data. Remote Sens. 12, Pp. 2949. https://doi.org/10.3390/rs12182949
- Boubaker Dhehibi, Shinan. N. Kassam, Aden Aw-Hassan, J.A.R., 2017. Enhancing agricultural extension services for rural development in Jordan. Int. J. Agric. Ext. 5, Pp. 51–60.
- Brutsaert, W., Sugita, M., 1996. Sensible Heat Transfer Parameterization for Surfaces with Anisothermal Dense Vegetation. J. Atmos. Sci. 53, Pp. 209–216. https://doi.org/10.1175/ 1520-0469(1996)053<0209:SHTPFS>2.0.CO;2
- Chakroun, H., Zemni, N., Benhmid, A., Dellaly, V., Slama, F., Bouksila, F., Berndtsson, R., 2023. Evapotranspiration in Semi-Arid Climate: Remote Sensing vs. Soil Water Simulation. Sensors 23, Pp. 2823. https://doi.org/10.3390/s23052823
- Chen, Y., Zhangwen Su, X.Z., 2024. The impact of climate change on water resources: Mechanism analysis, challenge assessment, and response strategies. Adv. Resour. Res. 4, Pp. 806–8018.https://doi.org/https://doi.org/10.50908/arr.4. 4_806
- Costa, J.M., Marques da Silva, J., Pinheiro, C., Barón, M., Mylona, P., Centritto, M., Haworth, M., Loreto, F., Uzilday, B., Turkan, I., Oliveira, M.M., 2019.
 Opportunities and Limitations of Crop Phenotyping in Southern European Countries. Front. Plant Sci. 10. https://doi.org/10.3389/fpls.2019.01125
- Degerli, B., Çetin, M., 2022. Using the Remote Sensing Method to Simulate the Land Change in the Year 2030. Turkish J. Agric. Food Sci. Technol. 10, Pp. 2453–2466. https://doi.org/10.24925/turjaf.v10i12.2453-2466.5555
- Denielle M. Perry, S.J.P., 2017. A New Era of Big Infrastructure?(Re) developing Water Storage in the US West in the Context of Climate Change and Environmental Regulation. Water Altern. 10.
- Derdar, B., 2011. Computing evapotranspiration of the olive and palm trees in Palmyra Oasis using remote sensing data within ALARM model. Damascus Univiversity.
- Elkatoury, A., Alazba, A.A., Radwan, F., Kayad, A., Mossad, A., 2024. Evapotranspiration Estimation Assessment Using Various Satellite-Based Surface Energy Balance Models in Arid Climates. Earth Syst. Environ. 8, Pp. 1347–1369. https://doi.org/10.1007/s41748-024-00501-1
- Hamaideh, A., Al-Zghoul, T., Dababseh, N., Jamrah, A., 2024. Enhancing Water Management in Jordan: A Fresh Tomato Water Footprint Analysis. Jordan J. Agric. Sci. https://doi.org/10.35516/jjas.v20i4.2571
- Hodgson, W.C., 2015. Food plants of the Sonoran Desert. University of Arizona Press..
- Houshang Ghamarnia, Davod Amirkhani, I.A., 2014. Basil (Ocimum basilicum L.) water use, crop coefficients and SIMDualKc model implementing in a semi-arid climate.. Int. J. Plant Soil Sci. 4, Pp. 535– 547.
- Jamrah, A., Al-Jawaldeh, H., Al-Zghoul, T.M., Hamaideh, Arwa, Darwish, M.M., Al-Karablieh, E., 2024. Olive Pits Activated Carbon As An Effective Adsorbent For Water Treatment Using H3po4 And H2so4 Activating Agents. Water Conserv. Manag. 8, Pp. 415–419. https://doi.org/http://doi.org/10.26480/wcm. 04.2024.415.419

- Kalua, M., Rallings, A.M., Booth, L., Medellín-Azuara, J., Carpin, S., Viers, J.H., 2020. sUAS Remote Sensing of Vineyard Evapotranspiration Quantifies Spatiotemporal Uncertainty in Satellite-Borne ET Estimates. Remote Sens. 12, 3251. https://doi.org/10.3390/rs12193251
- Koebele, E. A., and Simpson, K., 2023. The impacts of water scarcity on the security of democracies. In Handbook on Democracy and Security. Pp. 45-63. Edward Elgar Publishing. https://doi.org/10.4337/9781839100208.00010
- Kumar, N., Hamouda, M.A., 2025. Utility of single-source surface energy balance models in estimation of daily actual evapotranspiration in arid regions. Hydrol. Sci. J. https://doi.org/10.1080/02626667.2024.2446266
- Liang, S., Fang, H., Chen, M., 2001. Atmospheric correction of Landsat ETM+ land surface imagery. I. Methods. IEEE Trans. Geosci. Remote Sens. 39, Pp. 2490–2498. https://doi.org/10.1109/36.964986
- Meza, K., Torres-Rua, A.F., Hipps, L., Kopp, K., Straw, C.M., Kustas, W.P., Christiansen, L., Coopmans, C., Gowing, I., 2025. Relating spatial turfgrass quality to actual evapotranspiration for precision golf course irrigation. Crop Sci. 65. https://doi.org/10.1002/csc2.21446
- Owaneh, O.M., Suleiman, A.A., 2018. Comparison of the Performance of ALARM and SEBAL in Estimating the Actual Daily ET from Satellite Data. J. Irrig. Drain. Eng. 144. https://doi.org/10.1061/(ASCE)IR.1943-4774.0001335
- Pelgrum, W., Kuangmin Li, Smearcheck, M., van Graas, F., 2012. eDME architecture development and flight-test evaluation, in: 2012 IEEE/AIAA 31st Digital Avionics Systems Conference (DASC). IEEE, Pp. 1–37. https://doi.org/10.1109/DASC.2012.6383037
- Reints, J., Dinar, A., Crowley, D., 2020. Dealing with Water Scarcity and Salinity: Adoption of Water Efficient Technologies and Management Practices by California Avocado Growers. Sustainability 12, 3555. https://doi.org/10.3390/su12093555
- Sahoo, S.K., Goswami, S.S., 2024. Theoretical framework for assessing the economic and environmental impact of water pollution: A detailed study on sustainable development of India. J. Futur. Sustain. 4, Pp. 23– 34. https://doi.org/10.5267/j.jfs.2024.1.003
- Sejine, H., Anane, M., 2024. Remote sensing and GIS-based WetSpass-S model for estimating actual evapotranspiration in Grombalia region, Northeast Tunisia: comparison with ETLook WaPOR model. Euro-Mediterranean J. Environ. Integr. https://doi.org/10.1007/s41207-024-00628-7

- Slama, F., Zemni, N., Bouksila, F., De Mascellis, R., Bouhlila, R., 2019. Modelling the Impact on Root Water Uptake and Solute Return Flow of Different Drip Irrigation Regimes with Brackish Water. Water 11, Pp. 425. https://doi.org/10.3390/w11030425
- Smith, A., 2010. The theory of moral sentiments. Penguin.
- Sperling, O., Shapira, O., Tripler, E., Schwartz, A., Lazarovitch, N., 2014. A model for computing date palm water requirements as affected by salinity. Irrig. Sci. 32, Pp. 341–350. https://doi.org/10.1007/s00271-014-0433-5
- Suleiman, A., Al-Bakri, J., Duqqah, M., Crago, R., 2008. Intercomparison of Evapotranspiration Estimates at the Different Ecological Zones in Jordan. J. Hydrometeorol. 9, 903–919. https://doi.org/10.1175/2008JHM920.1
- Suleiman, A., Crago, R., 2002. Analytical land atmosphere radiometer model (ALARM) applied to a dense canopy. Agric. For. Meteorol. 112, Pp. 151–159. https://doi.org/10.1016/S0168-1923(02)00127-2
- Suleiman, A., Crago, R., 2004. Hourly and Daytime Evapotranspiration from Grassland Using Radiometric Surface Temperatures. Agron. J. 96, Pp. 384–390. https://doi.org/10.2134/agronj2004.3840
- Tan, S., Wu, B., Yan, N., Zeng, H., 2018. Satellite-Based Water Consumption Dynamics Monitoring in an Extremely Arid Area. Remote Sens. 10, 1399. https://doi.org/10.3390/rs10091399
- Trottier, J., Leblond, N., Garb, Y., 2020. The political role of date palm trees in the Jordan Valley: The transformation of Palestinian land and water tenure in agriculture made invisible by epistemic violence. Environ. Plan. E Nat. Sp. 3, Pp.114–14 0.https://doi.org/10.1177/2514848619876546
- Van, T.T., Tran, N.D.H., Bao, H.D.X., Phuong, D.T.T., Hoa, P.K., Han, T.T.N., 2017.
 Optical Remote Sensing Method for Detecting Urban Green Space as Indicator Serving City Sustainable Development, in: The 4th International Electronic Conference on Sensors and Applications.
 MDPI, Basel Switzerland, Pp. 140. https://doi.org/10.3390/ecsa-4-04932.
- Wu, Yongchuang, Wu, Yanlan, Wang, B., Yang, H., 2022. A Remote Sensing Method for Crop Mapping Based on Multiscale Neighborhood Feature Extraction. Remote Sens. 15, 47. https://doi.org/10.3390/rs15010047

